(Preprint) AAS 21-201

NUMERICAL PREDICTOR-CORRECTOR BASED GUIDANCE SCHEME FOR AERO-GRAVITY ASSIST AT TITAN FOR ENCELADUS MISSIONS

Daniel L. Engel[*], Soumyo Dutta[†], Zachary R. Putnam[‡]

Aero-gravity assist is a spacecraft manuever than can enable a vehicle to insert into an orbit of one planetary body using the atmosphere and gravity field of a secondary body, reducing the required propellant mass relative to a fully-propulsive orbit insertion. The Fully Numerical Predictor-Corrector Aerocapture Guidance algorithm was modified to work with a direct force control blunt body vehicle, executing an aero-gravity assist at Titan to enter a Saturnian orbit and conduct fly-by at Enceladus. Additionally, a proportional-integral-derivative controller was implemented to command sideslip angles for control of the orbital inclination. Numerical simulation showed the developed guidance scheme was capable of minimizing the energy and inclination error at atmospheric exit, allowing Saturnian moon tour trajectories and Enceladus exploration at a small delta-V cost, on the order of 100 m/s, in the nominal case.

INTRODUCTION

While Mars is one of the most common planetary locations for scientific missions, including the search for life, the Jovian and Saturnian moons also have the potential for major scientific discoveries and have gained the attention of mission planners and the scientific community. One example is Saturn's moon, Titan, which will be explored by the upcoming Dragonfly mission.[1] Titan has lakes of liquid ethane and methane, which are though to be part of a water-like cycle, potentially allowing for complex chemical processes, including life.[1,2] Another Saturnian moon, Enceladus, has drawn increasing study from the scientific community due to evidence of liquid water found by Cassini in 2015. Measurements of physical libration indicate the existence of a large liquid water sub-surface on Enceladus.[3] Enceladus also has interesting surface phenomena, including water vapor plumes, craters, and evidence of recent geologic activity.[4] Such findings make Enceladus an important candidate for future robotic exploration. The interplanetary trajectories required to reach Enceladus in a reasonable amount of time exhibit large hyperbolic excess velocities at arrival in the Saturnian system and require a large propellant mass fraction if existing chemical propulsion is used for a fully-propulsive insertion into a science orbit around Saturn for Enceladus observations.[5]

However, Titan's atmosphere may provide a suitable environment for performing various aeroassist maneuvers to reduce the propellant need for orbital insertion.[6] One example of an aeroassist

[*]Graduate Research Assistant, Department of Aerospace Engineering, University of Illinois at Urbana-Champaign, 104 S. Wright St., Urbana, IL 61801

[†]Aerospace Engineer, Atmospheric Flight and Entry Systems Branch, NASA Langley Research Center, MS 489, Hampton, VA 23681-2199.

[‡]Assistant Professor, Department of Aerospace Engineering, University of Illinois at Urbana-Champaign, 104 S. Wright St., Urbana, IL 61801

maneuver that may be enabling for Enceladus exploration is an aero-gravity assist, which involves a spacecraft utilizing a combination of Titan's gravitational forces and drag from its atmosphere in order to reduce the propellant mass fraction required for orbit insertion at Saturn. The aero-gravity assist may provide a significant portion of the velocity change and turn angle, δ, necessary to change the incoming orbit from a Saturn-centered hyperbolic orbit to an elliptical moon-tour orbit around Saturn.[6]

Successfully performing an aero-gravity assist maneuver, with minimal error, is a challenging problem that has yet to be demonstrated on a real mission. Variations in atmospheric and entry conditions have the potential to provide too much ΔV, resulting in the spacecraft capturing into an orbit around Titan or crashing into the surface. Alternatively, these uncertainties may result in too little ΔV, forcing the vehicle to expend additional propellant for correction maneuvers. Recent advances in guidance and control for planetary entry vehicles may provide potential solutions to the high degree of accuracy necessary to perform maneuvers like aero-gravity assist at Titan.[7] Numerical predictor-corrector guidance schemes do not rely on pre-determined reference trajectories but, instead, integrate the entry equations of motion on-the-fly to predict the end conditions; these guidance schemes have shown to be capable of accurately performing aeroassist maneuvers at a number of planetary bodies, including at Mars and the Ice Giants.[8,9] Furthermore, the improved accuracy of these guidance schemes may reduce the required control authority, allowing low lift-to-drag-ratio (L/D) vehicles to be used instead of new mid-L/D vehicles.[5,9]

Advanced guidance schemes may be further augmented by utilizing direct force control (DFC). DFC is an alternative to bank-angle modulation for steering during atmospheric flight. Instead of modulating the bank angle, DFC allows the vehicle angle of attack and sideslip angle to be independently modulated,[8] which enables independent control over the longitudinal and lateral channels and results in further control over flight performance. Control mechanisms like flaps[10] or differential geometry of the entry shape[11] could provide means to implement DFC. In this study, the focus is on the development and demonstration of a numerical predictor-corrector guidance scheme with a low-L/D DFC entry vehicle for aero-gravity assist at Titan. A guidance algorithm, originally developed for aerocapture, was modified to be compatible for aero-gravity assist. In aerocapture, the aero assist manuever is conducted about the planetary body where the spacecraft wants to attain the captured orbit; for aero-gravity assist, the manuever is conducted about one body (e.g. Titan) in order to attain a capture orbit about another body (e.g. Saturn). Results are assessed based on the accuracy of the guidance scheme in achieving the desired target conditions, the required command profiles, and the necessary propulsive correction maneuvers to obtain the correct orbit around Saturn.

MISSION DESIGN

This study considers a particular aero-gravity assist maneuver at Titan, designed to enable Enceladus exploration. The aero-gravity assist places the spacecraft on a "Moon Tour" orbit around Saturn that eventually leads to encounters with Enceladus. As part of recommendations to the Planetary Science Decadal Survey, Ref. 12 discusses several trajectories for Titan aero-gravity assist maneuvers for Enceladus observation in the 2040's. These trajectories have a variety of interplanetary trajectory end conditions for various choices of launch vehicles and spacecraft payload mass.

The particular aero-gravity assist trajectory considered in this paper is chosen due to its challeng-

ing flight environment, including a large Titan-relative V_∞* of 14.81 km/s, required in-atmosphere velocity change of approximately 12 km/s, and necessary turn angle of 33.96°.[7] The vehicle launches on a Delta IV Heavy class vehicle in 2033, arrives at the Saturnian system on a hyperbolic orbit on February 23rd, 2043, utilizing multiple Earth and Venus gravity assists in the process.[12] The concept of operations for the Titan aero-gravity assist is shown in Figures 1 and 2 for Saturn and Titan centered views, respectively. The vehicle enters Titan's sphere of influence (SOI) on a hyperbolic orbit with respect to both Saturn and Titan, with a Titan-relative V_∞ of 14.81 km/s. Entry interface at Titan's atmosphere occurs at an altitude of 1200 km. After a sensed acceleration magnitude of 0.1 Earth g, the vehicle begins active guidance, utilizing the numerical predictor-corrector guidance scheme described in the subsequent section. Active guidance continues until the spacecraft again reaches an acceleration magnitude below 0.1 g. After exiting Titan's atmosphere, the vehicle performs energy and orbit phasing propulsive correction maneuvers to further refine the moon tour trajectory. Over a 2.5 year period on the moon tour orbit, the spacecraft completes gravity assists among Saturn's inner moons, as well as propulsive maneuvers, which eventually allow the spacecraft to reach Enceladus for low energy fly-bys and scientific study.[12] The Titan atmospheric interface conditions for this particular trajectory are listed in Table 1, and the target orbital elements at atmospheric exit are listed in Table 2. The initial flight-path angle is chosen to optimize the aero-gravity assist maneuver and is discussed in the results section.

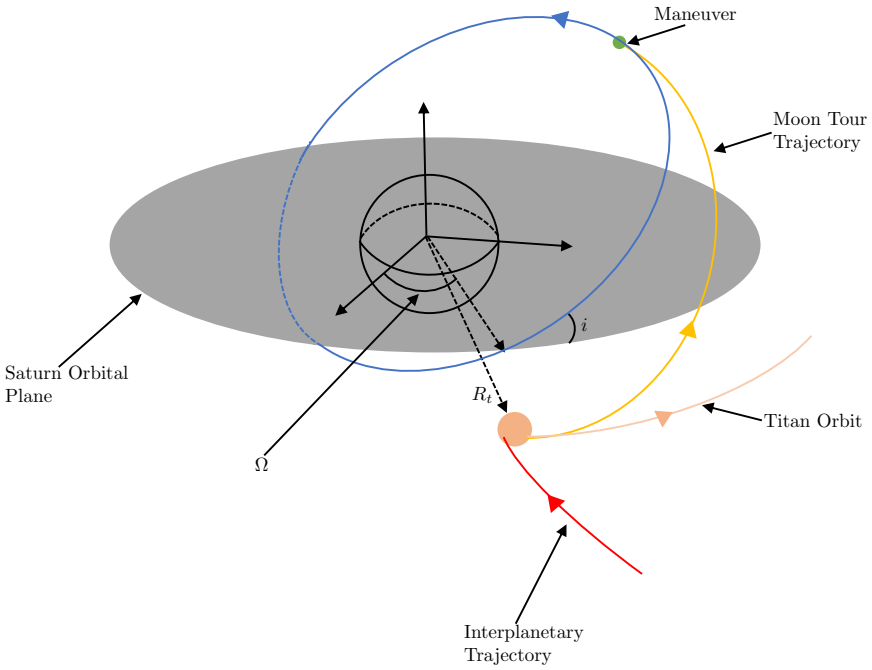

Figure 1: Saturn-centered view of aero-gravity assist

Accurately achieving the desired post-aero-gravity assist conditions requires real-time on-board guidance. The Fully Numerical Predictor-corrector Aerocapture Guidance algorithm (FNPAG) was the chosen guidance scheme for this study.[13] The Program to Optimize Simulated Trajectories II (POST2) was used to assess the flight performance of FNPAG during this aero-gravity assist trajectory by simulating both the guidance and trajectory of the spacecraft.[14] In these three degree-

*A section on mathematical notation is provided in the sequel.

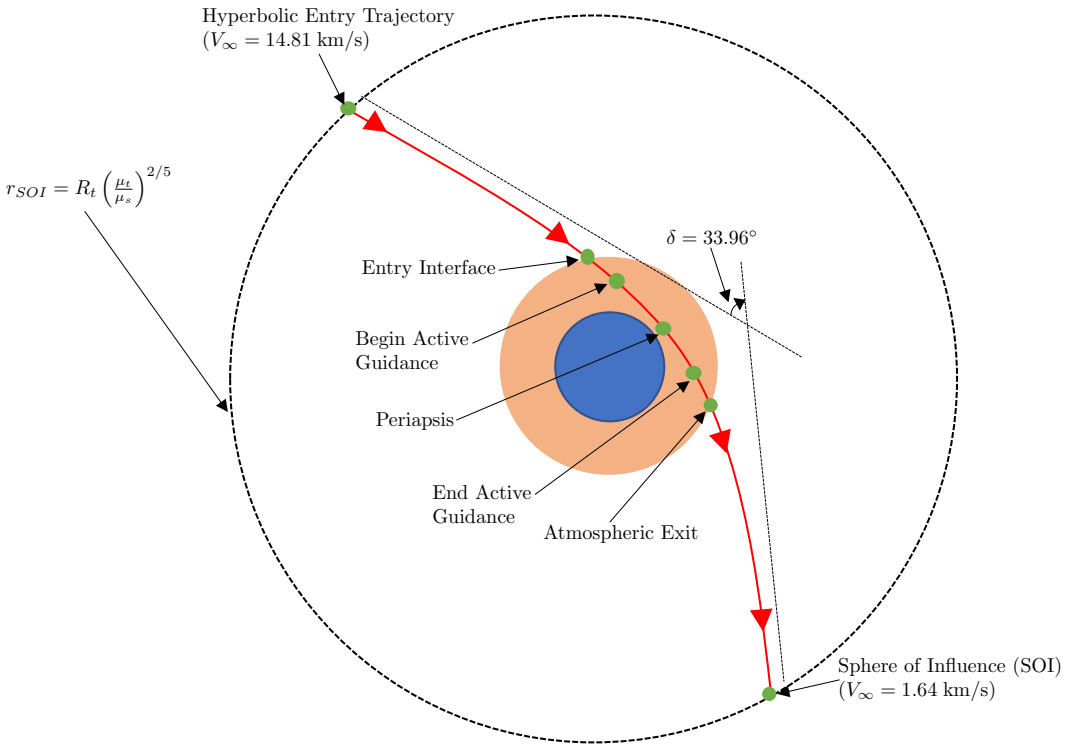

Figure 2: Titan-centered view of aero-gravity assist

Table 1: Entry conditions

Condition	Value
B-plane angle	-19.827°
V_∞	14.810 km/s
V_∞ right ascension	-1656.860°
V_∞ declination	148.374°
Entry interface altitude	1200 km
Time of flight	0.0 s

Table 2: Target conditions

Condition	Value
a_{des}	-3317.9 km
e_{des}	1.8525
i_{des}	144.6°
ω_{des}	102.613°
f_{des}	47.259°
Ω_{des}	18.628°

of-freedom (3-DOF) simulations, Titan was assumed to be a spherical body with a radius of 2574

km and a rotation rate $\Omega_{rot} = 4.561 \times 10^{-6}$ rad/s. The Titan 2004 Global Reference Atmospheric Model (GRAM) was used to determine the atmospheric conditions at a given altitude.[15]

Recent studies used to inform the Planetary Decadal Survey[12] of an aero-gravity assist at Titan have considered already existing aerodynamic shapes to minimize cost and risk. Thus, the vehicle for this study was assumed to be a low-L/D, 70° sphere-cone, with an outer radius of 2.25 m and nose radius of 1.125 m. The MSL aerodynamics database was used to determine the aerodynamic coefficients at a given α, β, and Mach number.[16] Sutton-Graves, cold-wall, stagnation-point heating with a constant of 1.7407×10^{-4} kg$^{1/2}$/m was used to assess heating in Titan's atmosphere.[17] The vehicle was also assumed to be capable of DFC, allowing the values of α and β to be independently modulated. A number of actuation methods are possible for DFC, including aerodynamic flaps,[10] moving mass systems,[18] and morphing vehicle structures.[11] While no specific actuation method was specified for this study, the vehicle was assumed to be able to modulate α and β with the conditions described in Table 3. The α and β modulation are subjected to rate and acceleration limits and are not assumed to be instantaneous to preserve the limitations of actual actuation systems. On-board navigation knowledge in this study was assumed to be perfect. In follow-up studies, the effect of navigation errors, especially characteristics like sensor biases and misalignments, will be addressed.

Table 3: DFC vehicle parameters

Parameter	Value
α_{max}	24°
β_{max}	5°
α_{min}	-24°
β_{min}	-5°
$\dot{\alpha}$	5°/s
$\dot{\beta}$	2°/s
$\ddot{\alpha}$	2°/s^2
$\ddot{\beta}$	0.3°/s^2

FULLY NUMERICAL PREDICTOR-CORRECTOR AEROCAPTURE GUIDANCE

Longitudinal Channel

The guidance algorithm used for the longitudinal channel in trajectory simulations for this study is an adaptation of the FNPAG algorithm, which was originally designed for bank-angle modulation. FNPAG is part of a broader class of numerical predictor-guidance schemes that rely on integrating the 3-DOF trajectory equations of motion from the current state in order to determine the appropriate actions needed to reach a desired target condition. The FNPAG command profile is based on optimal control, where the guidance follows a bang-bang solution for the bank profile, between the smallest and largest bank angles (0° and 180°).[13]

Since its earlier formulation, FNPAG has been adapted for DFC vehicles.[8,9] When adapted for DFC, the bang-bang α solution is not necessarily optimal in all circumstances, however the bang-bang solution can still be used to provide α commands.[8] To allow for robustness to atmospheric dispersions, the guidance scheme is split into two phases and is not solely limited to just the minimum and maximum α of the bang-bang solution.[8] In phase 1, the vehicle flies at a large, constant,

positive α. Using this negative angle results in negative lift, allowing the vehicle to fly lower into the atmosphere to generate the maximum amount of drag and ΔV. At every guidance cycle during phase 1, FNPAG calculates the switching time, t_s, when if the vehicle switched to a large negative α (now flying lift-up), it would achieve the minimum error in the targeting conditions. A graphical representation of the phase 1 α profile is shown in Figure 3. Once the actual guidance time reaches t_s, the guidance switches into phase 2. In phase 2, FNPAG modulates the α profile needed to reach minimum error in the target conditions during each guidance cycle.

For both phase 1 and phase 2, the calculations of t_s and the commanded α profile are done by solving for the minimum of a cost function each guidance cycle. This cost function varies depending on the application. In the case of aerocapture, where the goal is to attain a capture orbit around the atmospheric body where the aeroassist maneuver is occurring, the cost function is be the ΔV required during the correction burn at apoapsis.

FNPAG's formulation is such that it requires very few user-determined parameters in order to properly execute.[13] Examples of user-determined parameters include the solution convergence tolerances.

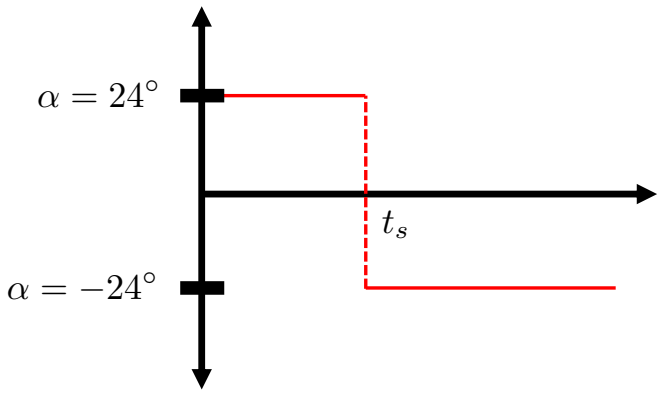

Figure 3: α profile during phase 1 of FNPAG

Aero-gravity assist differs from aerocapture and other aeroassist maneuvers in that the incoming and outgoing trajectories are hyperbolic with respect to the maneuvering body (e.g. Titan). Thus, there is no minimization parameter completely analogous to the ΔV correction for aerocapture. The degree of success of the aero-gravity assist, particularly for this moon tour problem, is largely related to the orbital energy after atmospheric exit from Titan; successfully achieving the desired moon tour orbit, with minimal correction burns, is dependent on the aero-gravity assist removing the correct amount of orbital energy. Thus, to adapt FNPAG for aero-gravity assist, the cost function to minimize is the error in specific orbital energy:

$$f(\alpha_{cmd}, t_s) = E_f - E_{des} = \left(\frac{V_f^2}{2} - \frac{\mu_t}{r_f}\right) - E_{des} \tag{1}$$

where, E_f is the predicted hyperbolic orbital energy at atmospheric exit of Titan, V_f is the predicted velocity at atmospheric exit, and r_f is the radius of atmospheric exit. E_{des} is the desired orbital energy at atmospheric exit and can be computed from the targeted semimajor axis in Table

2:

$$E_{des} = \frac{-\mu_t}{2a_{des}} = 1.353 \times 10^6 \text{ m}^2/\text{s}^2 \tag{2}$$

In the implementation of FNPAG used for this study, Equation (1) is minimized by using the Golden-section method. Each iteration of the Golden-Section requires a function evaluation with either t_s or α_{cmd}, depending on if the guidance is in phase 1 or phase 2. Evaluating Equation (1) involves integrating the 3-DOF equations of motion of a spacecraft in the atmosphere of a rotating spherical planetary body forward in time from the current position. In particular, these equations are:[9,13]

$$\dot{r} = V \sin\gamma \tag{3}$$

$$\dot{\theta} = \frac{V \cos\gamma \sin\psi}{r \cos\phi} \tag{4}$$

$$\dot{\phi} = \frac{V \cos\gamma \cos\psi}{r} \tag{5}$$

$$\dot{V} = -\frac{D}{m} - g \sin\gamma + \Omega_{rot}^2 r \cos\phi(\sin\gamma \cos\phi - \cos\gamma \sin\phi \cos\psi) \tag{6}$$

$$\begin{aligned} \dot{\gamma} = \frac{1}{V}\Bigg[\frac{L}{m} + (V^2/r - g)\cos\gamma + 2\Omega_{rot} V \cos\phi \sin\psi \\ + \Omega_{rot}^2 r \cos\phi(\cos\gamma \cos\phi + \sin\gamma \cos\psi \sin\phi) \end{aligned} \tag{7}$$

$$\begin{aligned} \dot{\psi} = \frac{1}{V}\Bigg[-\frac{S}{m\cos\gamma} + \frac{V^2}{r}\cos\gamma \sin\psi \tan\phi \\ + 2\Omega_{rot} V(\tan\gamma \cos\psi \cos\phi - \sin\phi) + \frac{\Omega_{rot}^2 r}{\cos\gamma} \sin\gamma \sin\phi \cos\phi\Bigg] \end{aligned} \tag{8}$$

Over the course of several iterations during each guidance cycle, values for t_s and α_{cmd} are determined and then commanded to the vehicle, allowing for targeting in the longitudinal channel. An α profile with several labeled FNPAG parameters, some of which are discussed in subsequent sections, is shown in Figure 4.

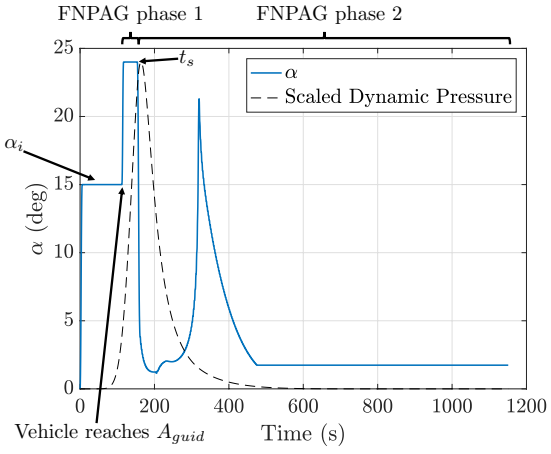

Figure 4: Sample α profile with labeled FNPAG parameters

Lateral Channel

While the longitudinal channel (i.e. α) is used to control the orbital energy, the lateral channel (i.e. β) is used to control the orbital inclination. Control over the lateral channel differs from the longitudinal channel, for this application, in that the initial inclination from the interplanetary trajectory is nearly the desired inclination. As a result, predictive control is not necessary, as was for the longitudinal channel. In the original formulation of FNPAG, lateral error was managed through bank reversals.[13] Implementations for FNPAG for aerocapture on DFC vehicles have used both β reversals[9] and proportional-integral-derivative (PID) controllers.[8] This study opted to use a PID controller due its ability to directly target the desired inclination while lowering control effort relative to β reversals, which may lead to over-corrections and excess control authority that could be used for the longitudinal channel. The PID controller is of the form:

$$\beta_{cmd} = K_p \left(i - i_{des}\right) + K_i \int_0^t (i - i_{des}) dt + K_d \frac{\mathrm{d}}{\mathrm{d}t} \left(i - i_{des}\right) \tag{9}$$

PID controller gains are shown in Table 4. These gains were tuned to create a balance between accuracy in achieving the desired inclination angle and to provide robustness to a range of γ_i and β_{veh}. Testing in the simulation also indicated that initiating lateral control at periapsis (i.e. $\gamma = 0^\circ$) further increased the robustness of the PID controller in targeting inclination. These simulations therefore had the vehicle fly at $\beta = 0^\circ$ prior to passing through periapsis.

Table 4: Gains for lateral PID controller

Gain	Value
K_p	-4.5
K_i	-0.005 s^{-1}
K_d	-100 s

NOMINAL FLIGHT PERFORMANCE

Flight-path Angle and Ballistic Coefficient Design Space

Initial mission-design space exploration was conducted using a lower-fidelity simulation to determine the ranges of γ_i and β_{veh} that may lead to a successful maneuver. This lower-fidelity simulation utilized the following bounding trajectories instead of active FNPAG guidance: full lift-up, full lift-down, lift-down from entry interface to periapsis; lift-up from periapsis to atmospheric exit, and lift-up from entry interface to periapsis; lift-down from periapsis to atmospheric exit. Each of these command-profile families were run from entry interface to atmospheric exit, for a grid of γ_i and β_{veh}, and Figure 5 shows the conditions where the actual and desired hyperbolic orbital energy at atmospheric exit coincided for each family. These results show for that for a given trajectory type, increasing ballistic coefficient requires a steeper value of initial flight-path angle in order to reach the desired energy condition. It can also be seen that for a given ballistic coefficient, as trajectories utilize more lift-down control, the necessary γ_i for achieving the desired energy state becomes shallower. Note that nearly any ballistic coefficient and flight-path angle combination located under a given profile's contour on Figure 5 will result in a vehicle capturing into an orbit around Titan or becoming a lander. This is due to the fact that the target E_{des} is relatively close to zero (i.e. nearly a parabolic orbit) and highlights the need for an active on-board guidance for aero-gravity assist.

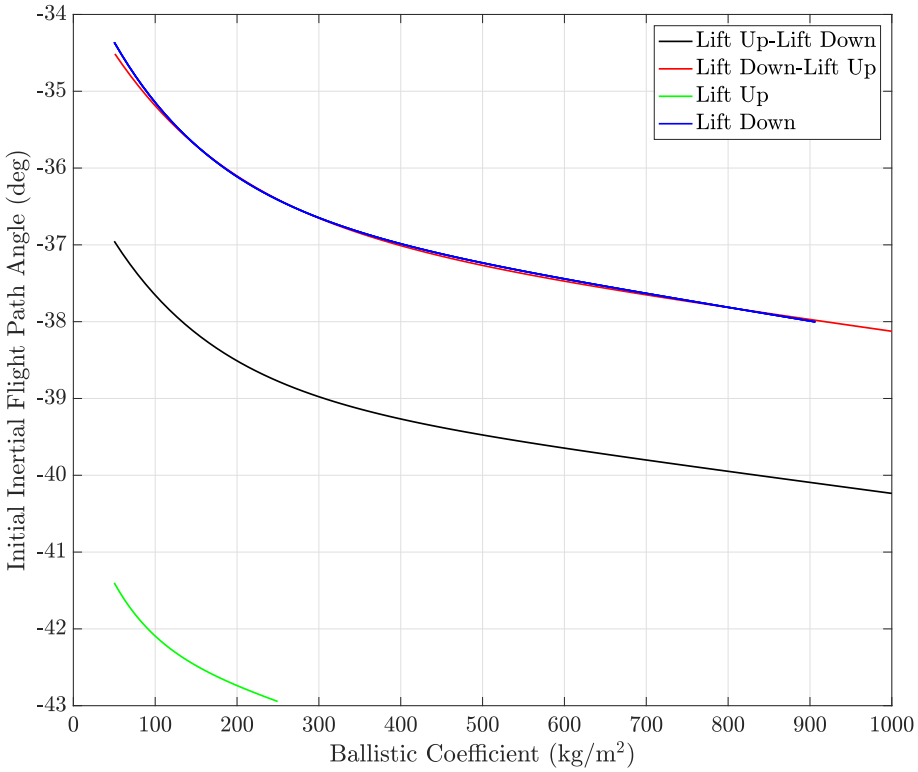

Figure 5: Design space of flight-path angles and ballistic coefficients for different trajectory types to reach desired exit energy state

Tuning Parameters

With an initial design space of γ_i and β_{veh} determined, trajectory analysis was performed in a more high-fidelity simulation in POST2, where the aerodynamic model and atmospheric models were not simplified, and the guidance scheme was FNPAG. The metric used to describe the effectiveness of a particular aero-gravity assist trajectory was the ΔV at Titan's SOI required to correct the resultant orbital energy error, post-aero-gravity assist. This parameter is both more intuitive in terms of mission design than just looking at the specific energy error and is analogous to the ΔV for the correction burn of an aerocapture maneuver at apoapsis. The calculation for ΔV at SOI is:

$$\Delta \mathrm{V}_{SOI} = \sqrt{2E + \frac{2\mu_t}{r_{SOI}}} - \sqrt{2E_{des} + \frac{2\mu_t}{r_{SOI}}} \tag{10}$$

where,

$$r_{SOI} = R_t \left(\frac{\mu_t}{\mu_s}\right)^{2/5} \tag{11}$$

The value of R_t in Eq. (11) corresponds to the Titan-Saturn distance. This ΔV at SOI is not only useful for assessing individual trajectories but also a method for tuning several guidance parameters that may lead to improved performance. One example of such a parameter is the guidance initiation

condition (A_{guid})—the sensed acceleration magnitude at which guidance starts during atmospheric flight. Performance was evaluated for A_{guid} values of 0.1 g, 1.0 g, and 2.0 g. Guidance should be started as soon as the vehicle possesses a measure of aerodynamic control authority. For all three cases, there was about a 0.3° range of γ_i that allowed for a ΔV at SOI of under 100 m/s for the nominal case. Outside of this range, the ΔV either grew very quickly or led to aerocapture or landing. The relationship between A_{guid} and the ΔV at SOI is shown in Figure 6a. While each case of A_{guid} was able to provide similar values for ΔV at SOI, using higher values of A_{guid} tended to increase the steepness of the necessary γ_i.

Furthermore, while larger values of A_{guid} did allow for reasonable ΔV at SOI, the use of these larger values mean the guidance waited longer to start, eventually leading to saturation of the α profile commanded to achieve the target conditions. The saturation in the α profile is demonstrated in Figure 6b. To preserve margin in the presence of other dispersions, the smaller threshold of $A_{guid} = 0.1$ g was chosen for this study.

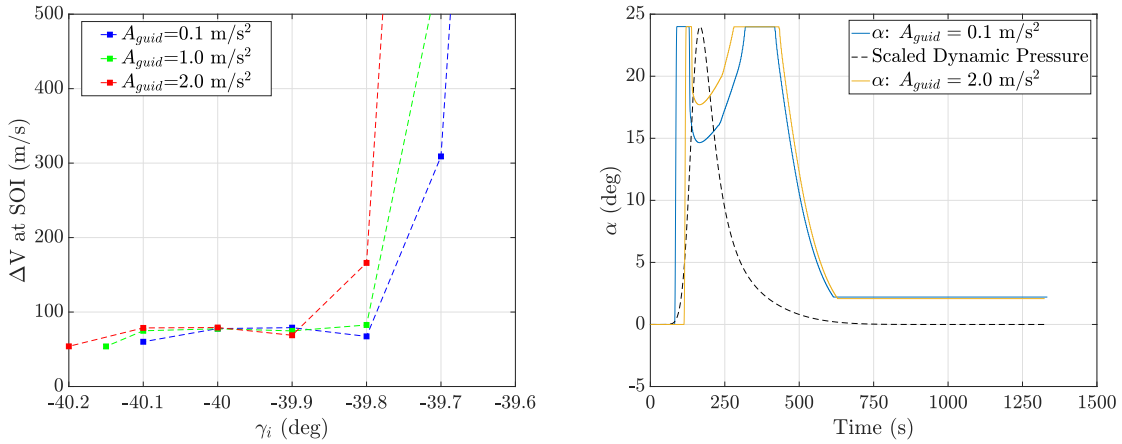

(a) (b)

Figure 6: Effect of changing values of A_{guid}: (a) ΔV at SOI as a function of γ_i and (b) Saturation of α profile.

Another tuning parameter assessed was the pre-guidance-initialization angle of attack (α_i), which is the angle flown by the vehicle prior to guidance start (i.e. prior to reaching a sensed acceleration equivalent to A_{guid}). The effect of α_i was assessed for values of 0° (i.e. no pre-guidance α), 15°, and 24° (which was the maximum α allowed). The relationship between the ΔV at SOI and γ_i, for the different values of α_i, is shown in Figure 7a. Similar to A_{guid}, for the different values of α_i considered here, a small ΔV at SOI can be achieved. For each α_i, there is approximately a 0.3° range of γ_i values in which the vehicle can achieve a ΔV at SOI under 100 m/s for the nominal case. The choice of α_i was not found to have a significant impact on saturation of the α command profile.

However, the choice of α_i did have an impact on the heating during flight. Plots of the peak heat flux and integrated heat load as a function of γ_i, for each of the values of α_i, are shown in Figure 7b and 7c. These results show that increasing α_i shifts the plotted contours to the right (i.e. shallower values of γ_i are needed). For the cases of ΔV at SOI and integrated heat load, the shift is horizontal, indicating that the choice of α_i does not change the ΔV and heat load value, just what γ_i is needed.

Increasing α_i, however, was found to shift the peak heat flux, both up and to the right, indicating that increasing α_i leads to higher peak heat flux. For this reason, as well as a zero α_i being more neutral to dispersions than other finite positive or negative values, α_i was chosen to be 0° for the remainder of the study.

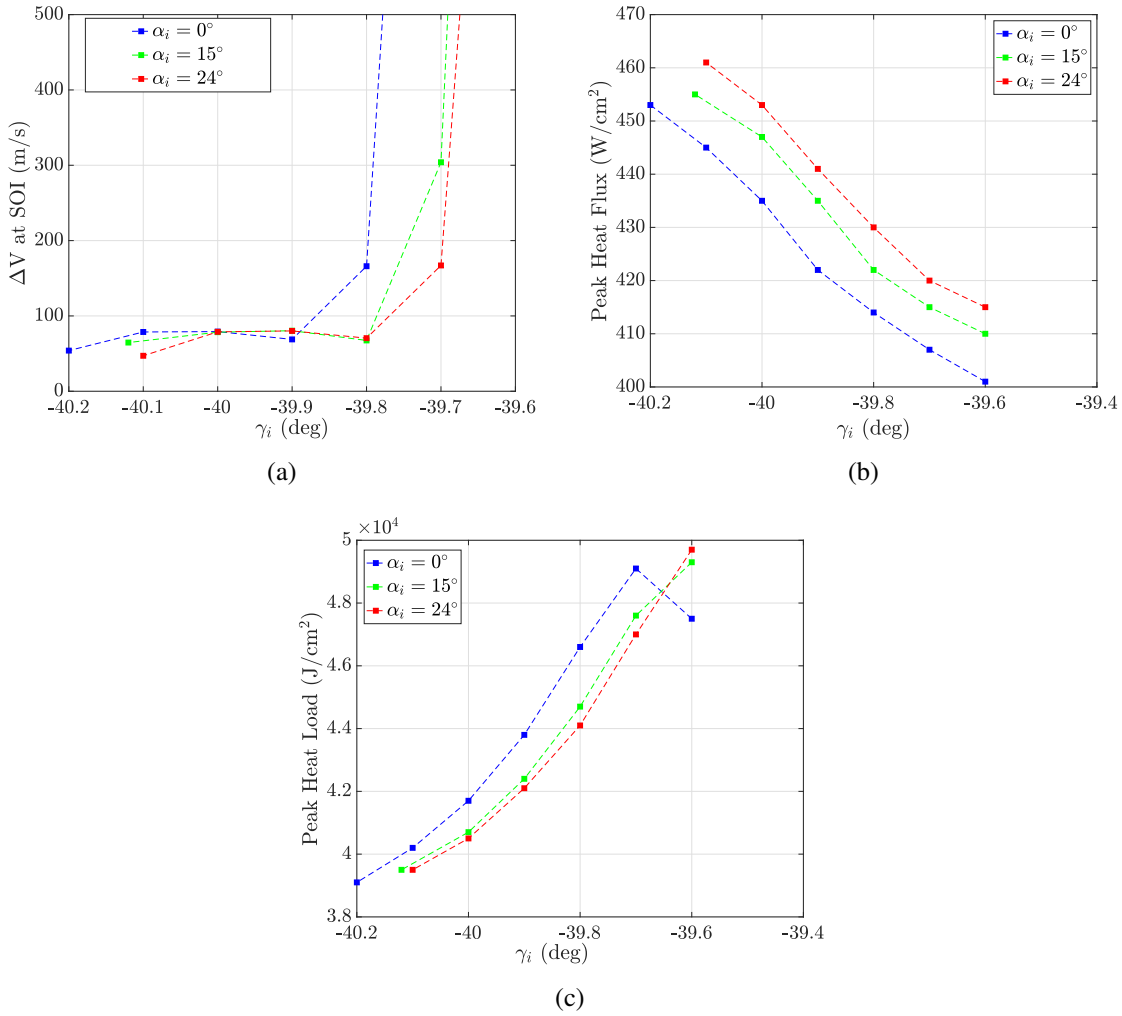

Figure 7: Effect of changing values of α_i: (a) ΔV at SOI as a function of γ_i, (b) Peak heat flux, and (c) Peak heat load

Target Trajectory

A target trajectory with FNPAG was run in POST2 with a γ_i of -40.2° and a β_{veh} of 150 kg/m^2 in order to demonstrate a "nominal" trajectory that achieves a desired, low ΔV at Titan SOI while not leading to α profile saturation. Trajectory data for this flight is shown in Figure 8. These plots show that the vehicle flies to a minimum altitude of approximately 260 km above Titan, allowing it to remove a significant portion of its initial velocity. In this particular case, while under 300 km, the vehicle achieves a ΔV of more than 9 km/s. In total, this aero-gravity assist trajectory provides a total in-atmosphere ΔV of 12.2 km/s and $\delta = 32.26^\circ$. Over the course of this trajectory, the vehicle

experiences a peak heat flux of 460.5 W/cm^2, an integrated heat load of 3.9×10^4 J/cm^2, and a peak acceleration magnitude of 14.5 g. Figure 8d shows the specific orbital energy as a function of time over the course of this trajectory.

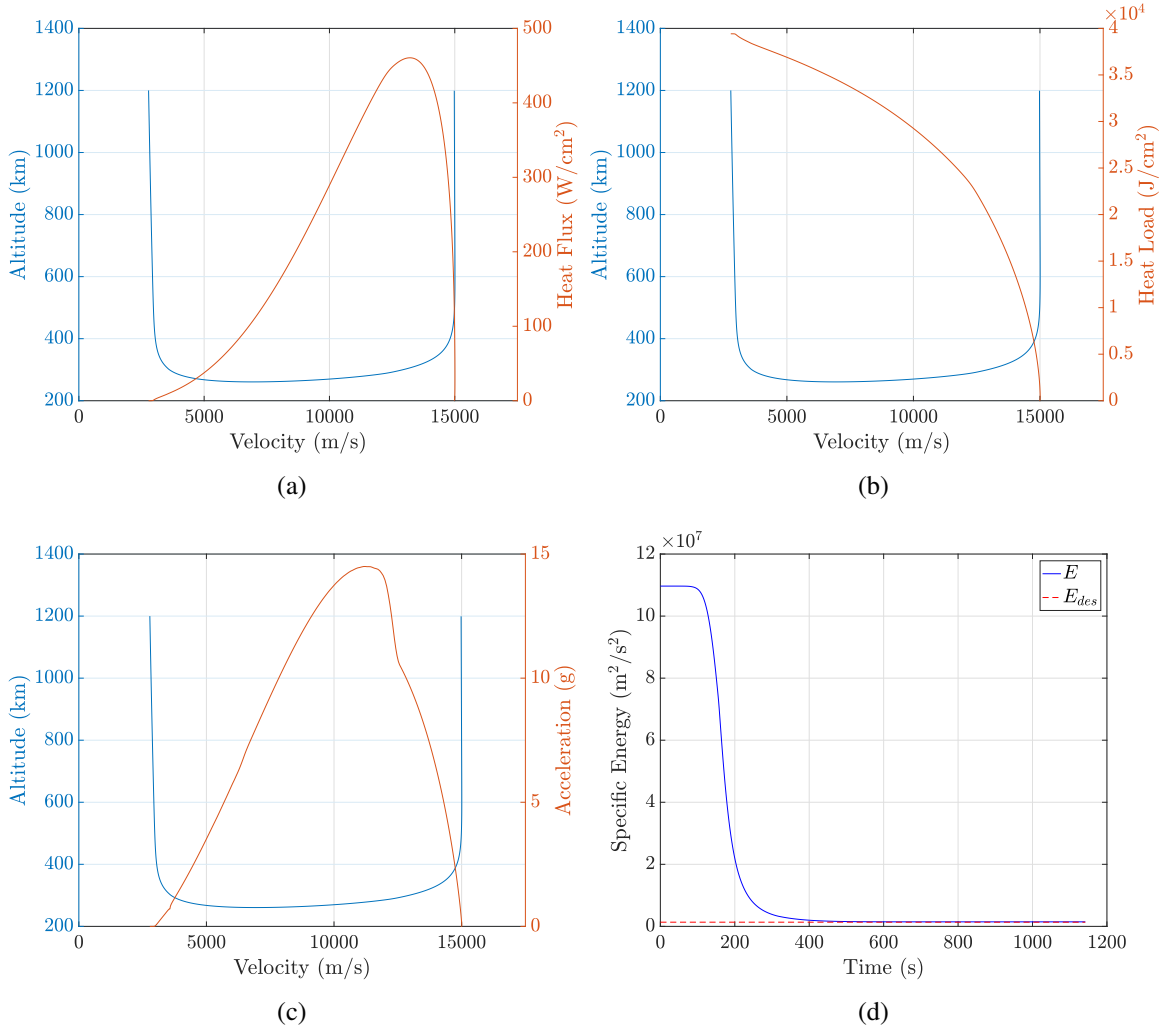

Figure 8: Trajectory data from sample aero-gravity assist run: (a) Altitude and heat flux as a function of velocity, (b) Altitude and integrated heat load as a function of velocity, (c) Altitude and acceleration as a function of velocity, and (d) Specific energy as a function of time

As discussed earlier, the desired orbital energy at atmospheric exit is close to zero, relative to the energy of the inbound trajectory. Figure 8d shows that the guidance scheme enables the vehicle to reach a final orbital energy very close to the desired value (7.8% error). The corresponding correction ΔV at Titan's SOI is 60.09 m/s. The α profile that enables this successful aero-gravity assist trajectory is shown in Figure 9. This plot shows that the α profile for this trajectory never saturates outside of phase 1, where the guidance, by design, commands the maximum control limit. In this particular α profile, the switch from phase 1 to phase 2 of FNPAG occurs around the time of maximum dynamic pressure, after which the α profile solution decreases near zero and then steadily increases until it reaches its maximum value. After reaching the maximum α value, the α profile

decreases until the guidance is terminated at 0.1 g, yielding a final value of 1.7°, which is held for the remainder of the flight, as expected in the design of FNPAG.

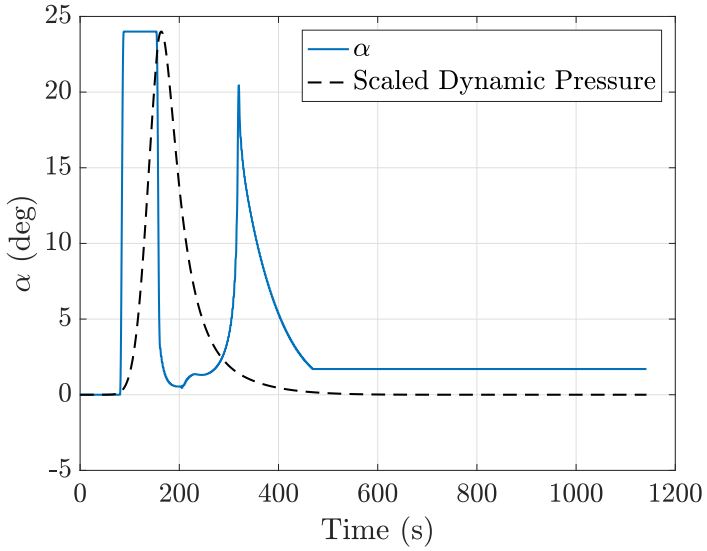

Figure 9: Angle of attack plotted as a function of time for example trajectory

The control over the inclination through β is shown in Figure 10. The commanded β remains at 0° until reaching $\gamma = 0^\circ$, which is the start of the lateral channel command. The PID controller then issues negative β commands which lead to an increase in the inclination angle. The commanded β initially saturates momentarily and then decreases to a value near -3° for the remainder of the flight. This controller results in an inclination error of -0.027°, which would require correction burns of less than 10 m/s. This indicates that this version of the FNPAG algorithm can work as a guidance scheme for a low L/D vehicle to successfully perform an aero-gravity assist at Titan for Enceladus exploration.

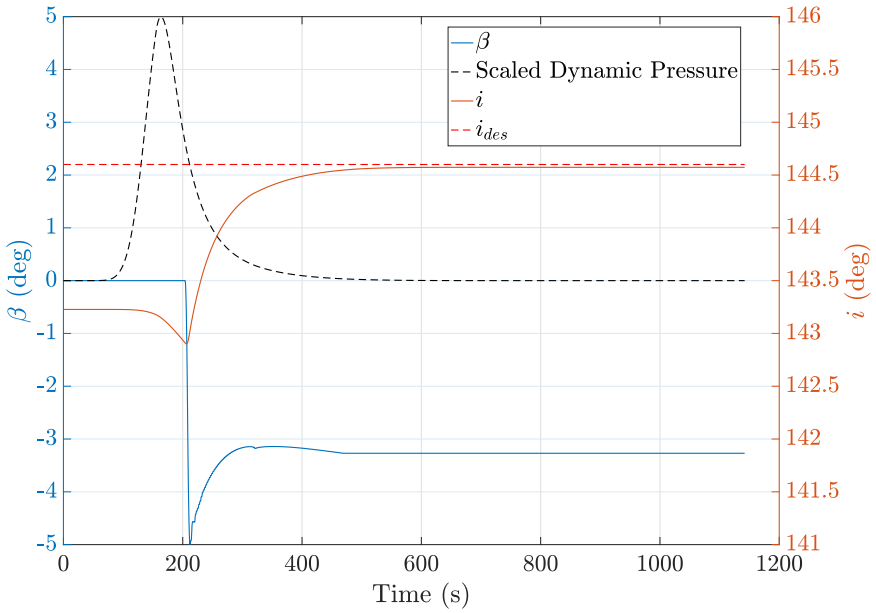

Figure 10: Sideslip and inclination angles plotted as a function of time

CONCLUSION

This study adapted the Fully Numerical Predictor-Corrector Aerocapture Guidance algorithm for a direct force control vehicle performing an aero-gravity assist at Titan. The guidance scheme was modified to use the error in orbital energy as the cost function to issue angle of attack commands and include a proportional-integral-derivative controller to issue sideslip angle commands to enable inclination targeting. In a nominal case, the adapted FNPAG algorithm allowed for much of the energy change needed for a Saturnian Moon Tour orbit, encountering Enceladus, without the need for a large propellant mass fraction. The proportional-integral-derivative controller was also able to correctly target the desired inclination without the need for large propulsive maneuvers. Actual implementation will likely require being able to target the orbital wedge angle, which consists of both the inclination and longitude of the ascending node. While this study considered the inclination, targeting of the full wedge angle, as well as an analysis robustness of this guidance scheme in the presence of dispersions, are important considerations for future studies.

NOTATION

a	=	orbital semimajor axis, km
A_{guid}	=	guidance initiation condition, m/s^2
D	=	drag force magnitude, N
e	=	orbital eccentricity
E	=	specific orbital energy, m^2/s^2
f	=	true anomaly, deg
g	=	acceleration due to gravity, m/s^2
i	=	orbital inclination, deg
K_d	=	derivative gain, s

K_i = integral gain, s^{-1}
K_p = proportional gain
L = lift force magnitude, N
m = vehicle mass, kg
r = Titan-relative position, km
R = Saturn-relative position, km
S = side force magnitude, N
t_s = switching time, s
V = planet-relative velocity magnitude, m/s
V_∞ = hyperbolic excess velocity, km/s
α = angle of attack, deg
α_i = pre-guidance-initiation angle of attack, deg
β = sideslip angle, deg
β_{veh} = vehicle ballistic coefficient, kg/m^2
δ = turn angle, deg
ΔV = velocity change, m/s
γ = inertial flight-path angle, deg
γ_i = initial, inertial flight-path angle, deg
θ = Titan-relative longitude, rad
μ = planetary gravitational parameter, km$^3/s^2$
ϕ = Titan-relative latitude, rad
ψ = heading angle, rad
ω = argument of periapsis, deg
Ω = longitude of the ascending node, deg
Ω_{rot} = Titan rotation rate, rad/s

Subscripts

cmd = commanded angle
des = desired value
f = value at atmoshperic exit of Titan
max = maximum
min = minimum
s = Saturn
SOI = sphere of influence
t = Titan

REFERENCES

[1] T. G. McGee, D. Adams, K. Hibbard, E. Turtle, R. Lorenz, F. Amzajerdian, and J. Langelaan, "Guidance, Navigation, and Control for Exploration of Titan with the Dragonfly Rotorcraft Lander," *2018 AIAA Guidance, Navigation, and Control Conference*, AIAA, 2018, 10.2514/6.2018-1330.

[2] M. Olivas, M. Gammill, and M. Hassanalian, "Conceptual Design of Fueling Mechanism for an Unmanned Aerial Vehicle with Harvesting Liquid-Methane Capability on Titan," *AIAA Aviation 2020 Forum*, AIAA, 2020, 10.2514/6.2020-2934.

[3] P. Thomas, R. Tajeddine, M. Tiscareno, J. Burns, J. Joseph, T. Loredo, P. Helfenstein, and C. Porco, "Enceladus's measured physical libration requires a global subsurface ocean," *Icarus*, Vol. 264, 2016, pp. 37–47, 10.1016/j.icarus.2015.08.037.

[4] A. Y. Lee, E. K. Wang, E. B. Pilinski, G. A. Macala, and A. W. Feldman, "Estimation and Modeling of Enceladus Plume Jet Density Using Cassini Flight Data," *Journal of Spacecraft and Rockets*, Vol. 50, No. 2, 2013, pp. 317–325, 10.2514/1.A32344.

[5] Y. Lu, *Planetay Mission Design and Analysis Using Aeroassist Maneuvers*. PhD thesis, Purdue University, 2019.

[6] T. Spilker, R. Moeller, C. Borden, W. Smythe, R. Lock, J. Elliott, J. Wertz, and N. Strange, "Analysis of Architectures for the Scientific Exploration of Enceladus," *2009 IEEE Aerospace Conference*, IEEE, 2009, 10.1109/AERO.2009.4839317.

[7] B. Tackett and e. al, "Guidance and Control Approaches that Enable Aerogravity Assist for an Enceladus Mission," *White Paper Submission for Planetary Science Decadal Survey, 2023 - 2032*, 2020.

[8] D. A. Matz and C. J. Cerimele, "Development of a Numeric Predictor-Corrector Aerocapture Guidance for Direct Force Control," *AIAA SciTech Forum*, AIAA, 2020, 10.2514/6.2020-0847.

[9] R. G. Deshmukh, D. A. Spencer, and S. Dutta, "Investigation of direct force control for aerocapture at Neptune," *Acta Astronautica*, Vol. 175, 2020, pp. 375–386, 10.1016/j.actaastro.2020.05.047.

[10] D. L. Engel, N. L. Skolnik, and Z. R. Putnam, "Configuration Options for Hypersonic Flaps for Mars Entry Systems," *AIAA SciTech Forum*, AIAA, 2021, 10.2514/6.2021-0933.

[11] A. D. Cianciolo, R. A. Lugo, A. M. Korzun, A. C. Slage, E. M. Queen, R. A. Dillman, and R. W. Powell, "Low Lift-to-Drag Morphing Shape Design," *AIAA SciTech Forum*, AIAA, 2020, 10.2514/6.2020-1266.

[12] J. Arnold and e. al, "Heatshields for Aerogravity Assist Vehicles Whose Deceleration at Titan Saves Mass for Future Flagship Class Exploration of Enceladus," *White Paper Submission for Planetary Science Decadal Survey, 2023 - 2032*, 2020.

[13] P. Lu, C. J. Cerimele, M. A. Tigges, and D. A. Matz, "Optimal Aerocapture Guidance," *Journal of Guidance, Control, and Dynamics*, Vol. 38, No. 4, 2015, pp. 553–565, 10.2514/1.G000713.

[14] R. W. Maddock, A. M. Dwyer-Cianciolo, D. Litton, and C. H. Zumwalt, "Insight Entry, Descent, and Landing Pre-Flight Performance Predictions," *AIAA SciTech Forum*, AIAA, 2020, 10.2514/6.2020-1269.

[15] A. L. Duvall, C. G. Justus, and V. W. Keller, "Global Reference Atmospheric Model (GRAM) Series for Aeroassist Applications," *43rd AIAA Aerospace Sciences Meeting and Exhibit*, AIAA, 2005, 10.2514/6.2005-1239.

[16] M. Schoenenberger, J. V. Norman, C. Karlgaard, P. Kutty, and D. Way, "Assessment of the Reconstructed Aerodynamics of the Mars Science Laboratory Entry Vehicle," *Journal of Spacecraft and Rockets*, Vol. 51, No. 4, 2014, pp. 1076–1093, 10.2514/1.A32794.

[17] Y. Lu and S. J. Saikia, "Feasibility Assessment of Aerocapture for Future Titan Orbiter Missions," *Journal of Spacecraft and Rockets*, Vol. 55, No. 5, 2018, pp. 1125–1135, 10.2514/1.A34121.

[18] B. M. Atkins and E. M. Queen, "Internal Moving Mass Actuator Control for Mars Entry Guidance," *Journal of Spacecraft and Rockets*, Vol. 52, No. 5, 2015, pp. 317–325, 10.2514/1.A32970.